# Noble-gas broadening rates for barium transitions involving the metastable $6s5d\ ^3D_J$ levels

E. Ehrlacher and J. Huennekens
*Department of Physics, Building 16, Lehigh University, Bethlehem, Pennsylvania 18015*
(Received 13 March 1992; revised manuscript received 3 June 1992)

The collisional-broadening rate coefficients, for both helium and argon buffer gases, have been measured for transitions from the metastable $6s5d\ ^3D_J$ levels in barium. A weak cw diode laser was used to populate the $^3D_J$ manifold through optical pumping of the $6s^2\ ^1S_0 \rightarrow 6s6p\ ^3P_1$ transition, followed by radiative decay into the $^3D_{2,1}$ states. The absorption coefficient for the transition of interest was then measured by monitoring the transmission of a very weak cw probe laser beam as its frequency was scanned over the line shape. Such scans were carried out for several diode (pump) laser powers, and using the standard line-shape normalization integral, we were able to construct density-independent line shapes. Each spectral line shape consists of many hyperfine components due to the presence of five barium isotopes (including two with nonzero nuclear spin). Each component is affected by Doppler, pressure, and natural broadening and, therefore, can be represented by a Voigt function. Thus, the measured line shapes (recorded with 50, 100, 200, and 500 Torr of either He or Ar buffer gas) were fitted with a sum of Voigt functions in which the only free parameter was the pressure-broadening rate. Using a least-squares fit of the broadening rates versus buffer-gas number density, the broadening-rate coefficients $k_{\rm br}$ were found. In addition, collisional line shifts for these transitions were measured, and shift rate coefficients $k_{\rm shift}$ were determined.

PACS number(s): 32.70.Jz

## I. INTRODUCTION

Line-shape studies have been of considerable interest in atomic physics because they provide information on fundamental long-range interactions between atoms. Line-shape studies of neutral barium have mainly concentrated on the $6s^2\ ^1S_0 \rightarrow 6s6p\ ^1P_1$ resonance transition at 553.5 nm [1–5]. Collisional-broadening rate coefficients (or, alternatively, cross sections) for the $6s^2\ ^1S_0 \rightarrow 6s6p\ ^1P_1$ resonance transition broadened by helium and argon perturbers were reported by Kuchta and co-workers in Ref. [5] and Penkin and Shabanova in Ref. [1]. Unfortunately, these numbers disagree by almost an order of magnitude.

The lowest metastable $6s5d\ ^{1,3}D_J$ levels in barium (see Fig. 1) also present an interesting area of study. Carlsten [6] has proposed that almost 80% of barium ground-state atoms can be optically pumped, through the $6s6p\ ^3P_1$ level, into these lowest metastable $^3D_J$ states. Since these levels are about 3000 $\rm cm^{-1}$ lower in energy than the nearest $P$ levels ($6s6p\ ^3P_J$) and radiative transitions back to the ground state are dipole forbidden, the lifetimes of atoms in these states are expected to be very long. Experimental evidence of this was provided by Schmelling [7], who determined a lower limit of 1 ms for the radiative lifetime of the metastable states from an atomic-beam magnetic-resonance experiment. In addition, Whitkop and Wiesenfeld [8], while studying quenching of the $6s5d\ ^3D_J$ levels, found significant population in the $^3D_3$ level up to 2 ms after firing their pulsed pump laser. Theoretical calculations by Migdalek and Baylis [9] have determined the lifetime of the $^3D_2$ state to be $\sim$60 sec. These are all consistent with observations made in our laboratory, where we have observed population in the metastable levels for at least a few hundred microseconds (this being a lower limit due to our detection system electronics) after the firing of a pulsed pump laser. In isotope-separation experiments, Bernhardt [10] has shown that, when pumping the $6s6p\ ^1P_1$ state, the $6s^2\ ^1S_0$ (ground) state for the $^{138}$Ba isotope was 97% depleted, with population presumably accumulating in the $6s5d\ ^1D_2$ metastable state. Klimovskii and co-workers [11] have measured the lifetime of the $^1D_2$ state to be 125 ms, while a recent calculation in Ref. [9] obtained a lifetime of 242 ms.

We are currently engaged in a series of experiments designed to study population and depopulation mechanisms of these metastable states using a variety of techniques. In this paper we report the results of an experiment to study collisions between excited barium atoms in the metastable $^3D_J$ levels and rare-gas (either helium or argon) perturbers. In particular, we have mapped out the line shapes and measured the collisional-broadening rate coefficients for the $6s5d\ ^3D_1 \rightarrow 5d6p\ ^1D_2^\circ$, $6s5d\ ^3D_2 \rightarrow 5d6p\ ^3F_3$, and $6s5d\ ^3D_3 \rightarrow 5d6p\ ^3F_4$ transitions using both He and Ar perturbers. Using a weak cw diode laser to pump the $6s^2\ ^1S_0 \rightarrow 6s6p\ ^3P_1^\circ$ transition (which populates the $^3D_{1,2}$ levels by spontaneous emission), we are able to produce a combined metastable-state density that is an appreciable fraction of the total barium number density. However, uncertainty in the determination of the ground-state number density does not allow us to make an accurate estimate of the fraction at this time. This uncertainty should be removed through a separate measurement which is currently under way in our laboratory.

The organization of the paper is as follows. In Sec. II we explain the experimental techniques used to measure

 ©1992 The American Physical Society

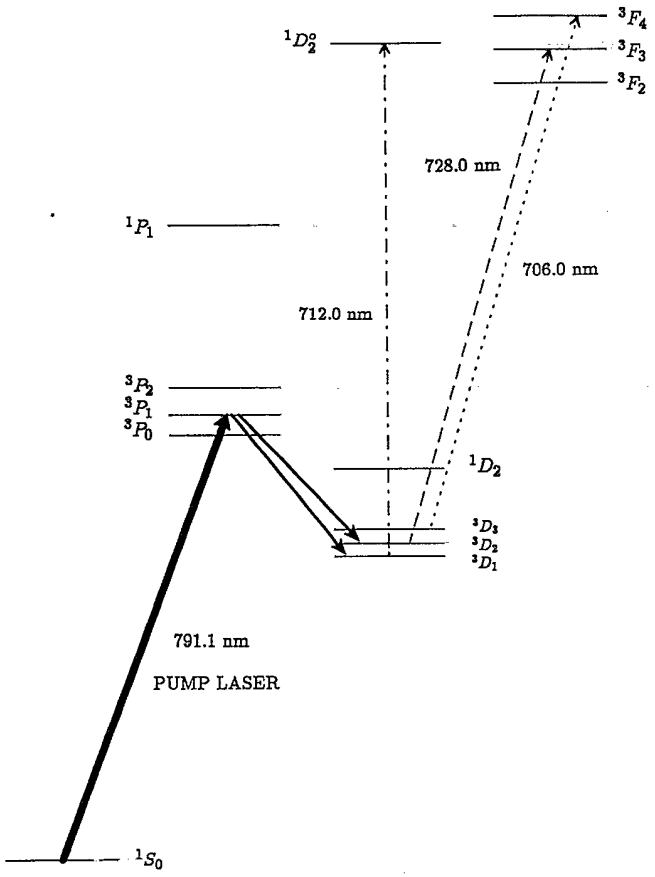


FIG. 1. Energy-level diagram of the lowest atomic levels in barium. The heavy solid arrow represents the pump laser, while the thin solid arrows represent the spontaneous emission channels which populate the metastable $^3D_J$ levels. The dashed lines denote the three probe laser transitions for which line shapes were measured in this experiment. Note that the level splittings for $^3D$ and $^3P$ are exaggerated for clarity.

the line shapes. A discussion of the method of data analysis is presented in Sec. III, including comments on hyperfine structure and isotope shifts. Also in Sec. III, the collisional-broadening rate coefficients are reported, along with a brief presentation of the line-shift data. Finally, in Sec. IV we present a discussion of sources of error in both the experiment and the analysis, followed by a few words regarding the relationship of this work to future experiments.

## II. EXPERIMENTAL METHODS

Figure 2 shows the experimental arrangement used in this investigation. Barium metal is contained in a 5-arm cross heat-pipe oven [12], which is typically heated to about 865 K. This results in a Ba vapor pressure of approximately 1 mTorr [13]. The oven also contains 50–500 Torr of either helium or argon as a buffer gas. Thus, the heat pipe is not operating in the true heat-pipe mode [14].

Barium ground-state atoms are optically pumped into the metastable $6s5d\ ^3D_J$ levels with a 20-mW, temperature- and current-tuned, $Al_{1-x}Ga_xAs$ diode laser tuned to the $6s^2\ ^1S_0 \rightarrow 6s6p\ ^3P_1^\circ$ intercombination line at 791.1 nm (see Fig. 1). Due to mirror losses, only about 15 mW of the laser power is incident on the barium vapor. The metastable $^3D_2$ and $^3D_1$ levels are populated by spontaneous emission from the $6s6p\ ^3P_1^\circ$ level. Once atoms reach the $^3D_J$ manifold, collisional mixing quickly redistributes population statistically over the $^3D_{1,2,3}$ levels. The populations of these metastable states are then probed in absorption using an argon-ion-laser-pumped, scanning, single-mode, ring-dye laser tuned to the following transitions (see Fig. 1):

$$6s5d\ ^3D_1 \rightarrow 5d6p\ ^1D_2^\circ \quad (712.03\ \text{nm}), \tag{1a}$$

$$6s5d\ ^3D_2 \rightarrow 5d6p\ ^3F_3 \quad (728.03\ \text{nm}), \tag{1b}$$

$$6s5d\ ^3D_3 \rightarrow 5d6p\ ^3F_4 \quad (705.99\ \text{nm}). \tag{1c}$$

These transitions were chosen because they all lie within the tuning curve of a single laser dye (pyridine-2 for our dye laser system), and the hyperfine structure of these transitions has been previously mapped out by others [7,15,16]. In order to avoid saturation and hyperfine pumping effects, the dye-laser beam is highly attenuated (a hundred nanowatts is typical for the power at the entrance to the heat-pipe oven). The dye-laser beam is chopped, and the transmitted dye-laser power is detected with a photomultiplier tube using lock-in detection. The diode- (pump) and dye- (probe) laser beams are counterpropagating and spatially overlapped in the heat-pipe oven. The diode-laser beam is collimated to an oval with approximate dimensions $5\times2$ mm$^2$. The dye-laser beam is unfocused and has a spot size of $\sim1$ mm. Thus, the region probed by the dye-laser beam is completely within the zone where the excited atoms are produced.

The diode-laser wavelength is tuned to the intercombination line by adjusting both the diode case temperature and the injection current, while simultaneously monitoring the dye-laser-beam absorption (with the dye-laser wavelength set to line center on one of the above transitions). To study the line-center region of the probe (dye-laser) transition, the diode-laser intensity is reduced, using neutral density filters, until the probe beam is $\sim50\%$ absorbed at line center. In other words, the metastable level populations are decreased, by reducing the pump intensity, to a point where the probe absorption is near 50%. The probe laser is then scanned over the transition while transmitted intensity as a function of frequency is recorded. It is important that this scan extend far enough into the line wings that an accurate baseline can be determined. Next, the dye laser is set to the frequency at which the absorption is about 20%. The diode- (pump) laser power is then increased (by removing neutral density filters) until the dye-laser beam (still tuned to the same frequency) is approximately 80% absorbed. The dye laser is once again scanned over the probe transition. With this procedure, a wide overlap region between these (or any) two consecutive scans is provided. This process of changing the diode power and scanning the probe laser frequency is repeated until the final scan is taken with full diode-laser-power incident on the barium vapor. Thus,

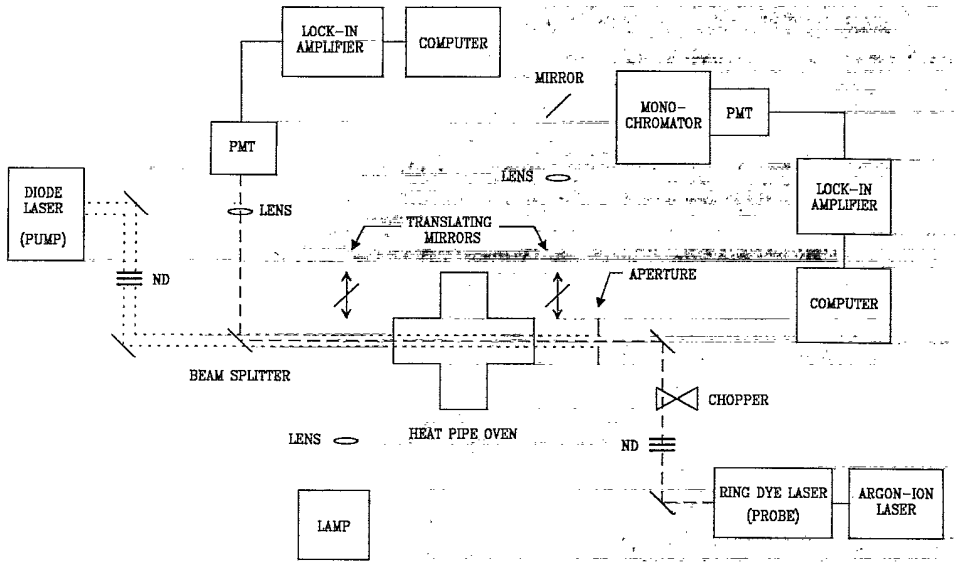


FIG. 2. Experimental setup. The diode- (pump) laser-beam path is denoted by the short-dashed lines, while the long-dashed line shows the probe-laser-beam path. Note that the pump beam has a larger diameter than the probe beam. Note also that by moving the translating mirrors into position in front of the heat-pipe oven windows, a white-light beam can be directed through the oven and into the monochromator. With this experimental configuration, the measurement of the ground-state number density by the absorption equivalent width method is possible. PMT, photomultiplier tube; ND, neutral density filters.

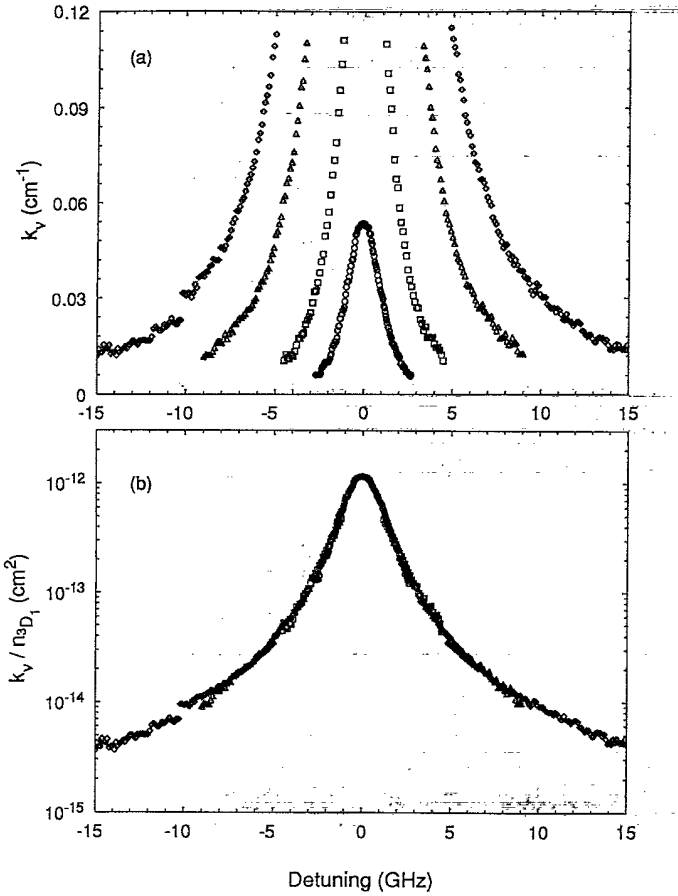


FIG. 3. Measured line shape for the $6s5d\ ^3D_1 \rightarrow 5d6p\ ^1D_2^\circ$ transition with 200 Torr of He buffer gas and an oven temperature of 873 K: (a) Probe-laser absorption scans for varying pump-laser power [15.5 mW (◇), 2.8 mW (△), 0.60 mW (□), 0.12 mW (○)]. Note that these traces have already been converted into $k_\nu = -(1/L)\ln[I_\nu(L)/I_\nu(0)]$, with only the 10–90% absorption regions shown in the figure. (b) Density-independent, fully normalized line-shape function produced from the data in (a).

the full line shape of the probe transition is progressively mapped from the core out to the line wings. At this point, a few scans with lower incident diode-laser powers are repeated in order to verify that possible drift of the diode-laser wavelength has not appreciably changed the probe laser absorption profile. Occasionally, the diode laser undergoes a mode hop, in which case the intercombination transition must be found again, and the full set of scans must be repeated.

The procedure outlined here was carried out for each of the lower metastable $^3D_J$ states, for both helium and argon buffer gases, and at pressures of 50, 100, 200, and 500 Torr. Figure 3(a) shows a full set of probe laser scans of this type, with varying diode-laser (pump) power, for the $6s5d\ ^3D_1 \rightarrow 5d6p\ ^1D_2^\circ$ transition with 200 Torr of He buffer gas in the heat pipe. It should be noted that the ground-state density was measured before and after each series of scans representing a given transition, buffer gas, and pressure. The $6s^2\ ^1S_0 \rightarrow 6s6p\ ^1P_1^\circ$ absorption at 553.5 nm was monitored using a white-light source and monochromator (see Fig. 2), and the ground-state atom density was then determined from the equivalent width method [17,18].

## III. ANALYSIS AND RESULTS

For a given set of ring-laser scans, corresponding to a particular transition with a particular buffer-gas species and pressure [as shown in Fig. 3(a)], a single composite line-shape function can be mapped [Fig. 3(b)]. These line shapes are then fitted to a Voigt function from which the barium-noble-gas collisional-broadening rate coefficients $k_{br}$ are determined.

To produce a composite line shape, the following procedure is used. First, the ring-laser absorption scans, which measure the probe laser intensity transmitted through the vapor as a function of frequency $[I_\nu(L) \equiv I_\nu(0)e^{-k_\nu L}$, where $I_\nu(0)$ and $I_\nu(L)$ are the incident intensity and the intensity transmitted through a

length $L$ of the vapor (at a frequency $\nu$), respectively], are converted to curves of $k_\nu$ versus $\Delta\nu$. Here, $\Delta\nu$ is the probe laser detuning from line center. In order for the absorption coefficient $k_\nu$ to be measured accurately in any region of the line, it is necessary for the total probe laser absorption in that part of the line to lie in the range 10–90 %. In the limit where self-broadening effects can be neglected, the absorption coefficient at all frequencies is proportional to the density of atoms in the lower state of the transition. Since in our experiment the lower state ($^3D_J$) density is controlled by the pump (diode-) laser intensity, we can guarantee that the probe laser absorption in any region of the line is in the 10–90 % range by simply varying the diode-laser intensity. Thus, by increasing the diode-laser intensity, the regions of the line shape which lie progressively farther in the line wings can be studied. Moreover, since the only thing that changes between members of a set of scans of this type is the diode-laser intensity and therefore, the lower ($^3D_J$) state density (which is proportional to $k_\nu$), it is easy to find a scaling factor between two successive scans $i$ and $j$, i.e., we find the average value of $(k_\nu)_j/(k_\nu)_i$ (denoted by $\langle\ \rangle_{\rm av}$) in the regions where the two scans overlap with reasonable signal-to-noise ratios:

$$f_{ij}\equiv\left\langle\frac{(k_\nu)_j}{(k_\nu)_i}\right\rangle_{\rm av}=\frac{(n_{^3D_J})_j}{(n_{^3D_J})_i}\ . \tag{2}$$

Here, $n_{^3D_J}$ is the number density in the particular $^3D_J$ level being probed. [Note that the metastable populations should increase linearly with pump laser power, in the low-power limit. For the conditions of our experiment, we indeed find the scaling factors obtained from Eq. (2) are in good agreement with the ratios of the incident diode-laser powers for each pair of scans.] Although we are able to obtain the relative lower-state densities between two scans in this fashion, we do not know the absolute $^3D_J$ level number densities for any of the scans at this point. Nevertheless, we can use the scaling factors $f_{ij}$ to create a single plot of $(k_\nu)_j/f_{ij}$ (which is equivalent to $k_\nu/n_{^3D_J}$ in relative units) for the full line shape.

Integration of this composite curve allows us to apply the well-known normalization condition [18]

$$\int\frac{k_\nu}{n_{^3D_J}}d\nu=\frac{\lambda^2}{8\pi}\frac{g_2}{g_1}\Gamma_{\rm nat} \tag{3}$$

to place the full line-shape function $(k_\nu/n_{^3D_J})$ on an absolute scale. Here, $\lambda$ is the transition wavelength; $g_1$ and $g_2$ are the lower- and upper-state statistical weights, respectively; and $\Gamma_{\rm nat}$ is the spontaneous emission rate of the transition. An example of such a curve constructed from the data in Fig. 3(a) is shown in Fig. 3(b). Note that once this final curve is constructed, the density of the lower state of the transition can be found for any pump laser intensity by comparing a measured $k_\nu$ value with the constructed $k_\nu/n_{^3D_J}$ curve.

In order to extract information on the collisional broadening of the transition, the composite line shape is then fitted to a Voigt function [19], which is a numerical convolution of a Gaussian and a Lorentzian function:

$$\frac{k_\nu}{n_{^3D_J}}=\frac{\lambda^2}{8\pi^2}\frac{g_2}{g_1}\frac{\Gamma_{\rm nat}}{\sqrt{\pi}}\frac{a}{\Delta}\int_{-\infty}^{\infty}\frac{e^{-y^2}}{(x-y)^2+a^2}dy\ , \tag{4}$$

with

$$x=\frac{\nu-\nu_0}{\Delta}\ , \tag{5a}$$

$$a=\frac{\Gamma_L}{4\pi\Delta}\ , \tag{5b}$$

$$\Delta=\frac{\Delta\nu_D}{2\sqrt{\ln 2}}\ , \tag{5c}$$

and

$$\Delta\nu_D=\frac{2\nu_0}{c}\left[\frac{2(\ln 2)kT}{M}\right]^{1/2}\ . \tag{5d}$$

Here, $a$ is the dimensionless Voigt parameter and $\Gamma_L$ is the Lorentzian component full width at half maximum (FWHM) in angular frequency units. The Lorentzian FWHM is related to the collisional-broadening rate $\Gamma_{\rm br}$ by $\Gamma_L=\Gamma_{\rm br}+\Gamma_{\rm nat}$. $\Delta$ is proportional to the Doppler (Gaussian) width $\Delta\nu_D$ [Eq. (5d)], where $\nu_0$ is the transition frequency and $T$ and $M$ are the temperature and barium atomic mass, respectively [18,19]. The normalization of the Voigt function is given by Eq. (3) and since the Doppler width is fixed by the temperature (which was not varied in the experiment), the only parameter which must be fitted is the Voigt parameter $a$, which is proportional to the Lorentzian width.

The situation described above is complicated somewhat by the hyperfine structure (hfs) of the transition under consideration. In particular, barium has five natural-

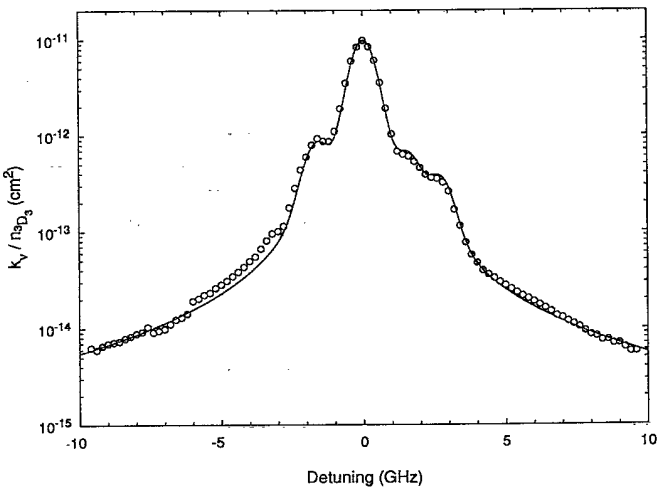


FIG. 4. Experimental line shape (○) for the $6s5d\ ^3D_3\rightarrow 5d6p\ ^3F_4$ transition, at 864 K, with 50 Torr of Ar buffer gas, showing the hyperfine structure. The solid line is the fitted line shape (composed of eight Voigt components).

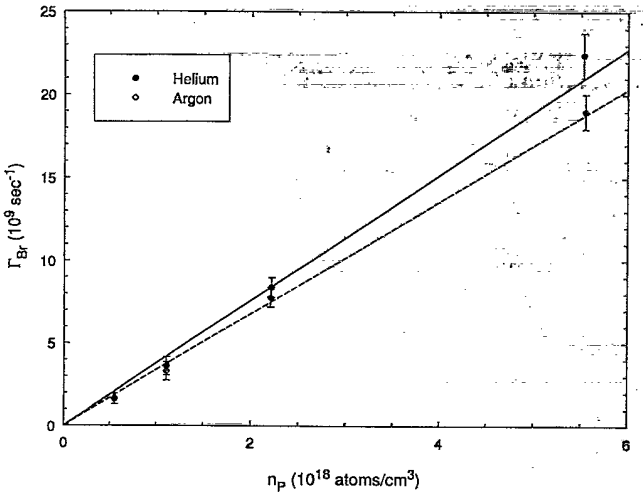


FIG. 5. Plot of $\Gamma_{br}$ vs perturber density $n_p$ for the $6s5d\ ^3D_2 \rightarrow 5d6p\ ^3F_3$ transition with He (●) and Ar (◇) perturbers. The solid and dashed straight lines are the least-squares fits for He and Ar buffer gas, respectively. Slopes of these lines yield $k_{br}$.

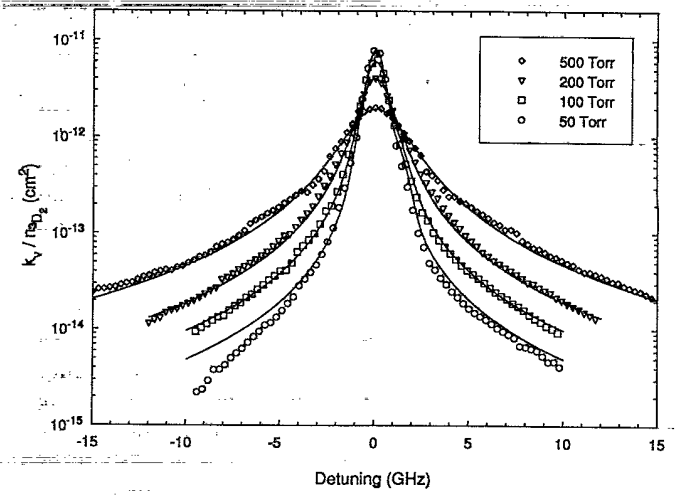


FIG. 6. Comparison of experimental $6s5d\ ^3D_2 \rightarrow 5d6p\ ^3F_3$ transition line shapes (data points) at various Ar pressures with full line shapes that were recalculated using the "best value" $k_{br}$ (solid lines). Line shifts have been suppressed in the figure.

ly occurring isotopes with abundances [illegible]. The even atomic number isotopes of barium ([illegible]Ba) constitute approximately 82% of the natural abundance with $^{138}$Ba as the major contributor at 71.7%. The even isotopes all have nuclear spin $I=0$ and, therefore, no level splitting (although there is still a small isotope shift). The odd isotopes ($^{137,135}$Ba), which contribute 17.8% to the total abundance, have nuclear spin $I=\frac{3}{2}$ and, thus a fourfold splitting of all levels of interest (threefold splitting for levels with $J=1$) in addition to isotope shifts. While the inclusion of the hfs of the transition is not required to fit the line wings which contain most of the information on the collisional broadening, it is required to fit the core. For data taken at 200 and 500 Torr, hfs structure is not noticeable because the pressure broadening is larger than the hyperfine splittings. But at the lower pressures, hyperfine structure is clearly evident, particularly for the $6s5d\ ^3D_3 \rightarrow 5d6p\ ^3F_4$ line shape which exhibits the largest level splittings (see Fig. 4). Thus, in order to obtain a better fit in both the line core and line wings, we decided to fit the experimental line shapes with a sum of Voigt functions representing the hyperfine structure and isotope shifts. We took hfs constants from Refs. [7,15,16]. Isotope shifts for each of the three transitions of interest were also reported in Ref. [16]. The line shapes were then fit to a sum of Voigt functions with the Voigt parameter $a$ as the only free parameter. The number of Voigt functions used in the fit depended on the transition, with components lying within 50 MHz being combined into single components. (Components contributing $<0.5\%$ of the total line strength were neglected.)

From the best fit of the composite Voigt function to the experimental line-shape function $k_\nu / n_{^3D_J}$, we obtain a best value of $\Gamma_{br}$ for a particular transition, noble-gas species, and pressure. Finally, we use the fact that

$$\Gamma_{br} = n_p k_{br} , \tag{6}$$

where $n_p$ is the noble-gas (perturber) number density, to determine $k_{br}$ for each transition (for both He and Ar perturbers). Using a least-squares fit, $k_{br}$ is found from the slope of $\Gamma_{br}$ versus noble-gas number density (see Fig. 5). Note that in Eq. (6) above we have neglected contributions to $\Gamma_{br}$ from collisions of Ba($^3D_J$) atoms with either ground-state or other excited-state barium atoms, since the noble-gas number density is approximately five orders of magnitude larger than the barium number density. The straight-line dependence of $\Gamma_{br}$ on the noble-gas number density seen in Fig. 5 demonstrates that this is a good approximation. The collisional-broadening rate coefficients for all three transitions, and for both buffer gases, are given in Table I. These "best value" broadening coefficients were then used to recalculate full compos-

TABLE I. Collisional-broadening and -shift rate coefficients (in units of $10^{-9}$ cm$^3$ sec$^{-1}$), measured at $T=865$ K, for barium transitions involving the metastable $6s5d\ ^3D_J$ levels. Note: $k_{shift}=2\pi\Delta\nu_{shift}/n_p$, with $\Delta\nu_{shift}$ the line-center shift in Hz.

| Transition | Helium | | | Argon | | |
|---|---|---|---|---|---|---|
| | $k_{br}$ | $k_{shift}$ | $k_{br}/k_{shift}$ | $k_{br}$ | $k_{shift}$ | $k_{br}/k_{shift}$ |
| $6s5d\ ^3D_1 \rightarrow 5d6p\ ^1D_2^\circ$ | 3.86±0.32 | 0.96±0.16 | +4.0±1.0 | 3.30±0.24 | −1.48±0.15 | −2.2±0.4 |
| $6s5d\ ^3D_2 \rightarrow 5d6p\ ^3F_3$ | 3.79±0.33 | 0.74±0.15 | +5.1±1.5 | 3.39±0.28 | −1.55±0.14 | −2.2±0.4 |
| $6s5d\ ^3D_3 \rightarrow 5d6p\ ^3F_4$ | 3.83±0.35 | 0.74±0.14 | +5.2±1.5 | 3.64±0.30 | −1.34±0.15 | −2.7±0.5 |

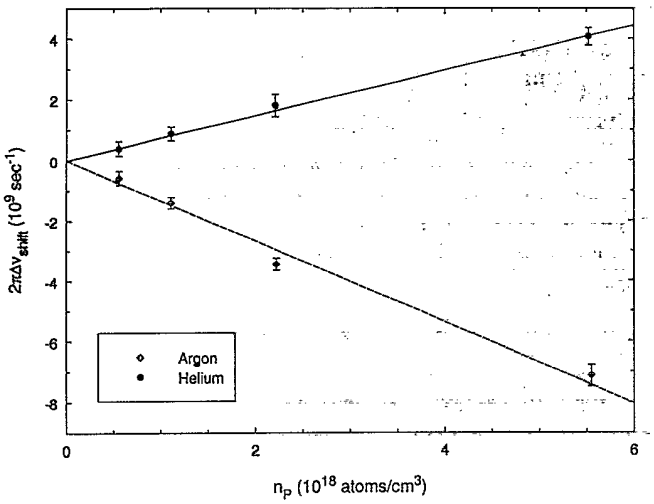


FIG. 7. Plot of line shift vs perturber density $n_p$ for the $6s5d\ ^3D_3 \rightarrow 5d6p\ ^3F_4$ transition with He (●) and Ar (◇) perturbers. The solid and dashed straight lines are the least-squares fits for He and Ar buffer gas, respectively. Slopes of these lines yields $k_{shift}$.

ite Voigt line shapes, which were compared to the measured line shapes, in order to show that the broadening rates are reasonable (see Fig. 6). We note that a $T^{0.3}$ temperature dependence of the rate coefficient $k_{br}$ is predicted for van der Waals broadening, while other types of interactions produce different temperature dependences [17]. Since temperature was not varied in our experiment, the values reported in Table I should be considered as valid for $T = 865$ K.

We also measured the line-center shifts $\Delta\nu_{shift}$ of the transitions due to collisions of the barium with different perturber gas species. Figure 7 shows the measured shifts for the $6s5d\ ^3D_3 \rightarrow 5d6p\ ^3F_4$ transition, as a function of buffer-gas density, for both He and Ar perturbers. Least-squares straight-line fits of the shift versus perturber number density yield the collisional-shift rate coefficients $k_{shift}$, which are also given in Table I. For all the transitions studied, helium perturbers were observed to cause a blueshift, while argon perturbers were found to produce a redshift. For a pure van der Waals interaction, it can be shown that the ratio of the collisional-broadening-to-shift rate coefficients is $-2.8$ (see Ref. [21] for an excellent recent example of an analysis of broadening-to-shift ratios in terms of different interactions). Table I gives the values of this broadening-to-shift ratio derived from our data. It can be seen that while the ratios for argon perturbers are reasonably close to the theoretical value predicted for van der Waals broadening, the helium data clearly cannot be described by a pure $1/R^6$ interaction. This is similar to the recent results of Ref. [21] for the resonance lines of lead.

## IV. DISCUSSION

Several sources of error are present in the analysis and will be discussed below. One source of error is the initial conversion of the ring-laser absorption profile into the absorption coefficient $k_\nu$. The error here is associated with the uncertainty in the baseline, which may be at most a few percent. In addition, the uncertainty in the vapor length $L$ (~20% for the nonequilibrium heat-pipe oven) contributes to the uncertainty in determination of both ground- and excited-state atom number densities, but not in the determination of the broadening rates. The same is true of the uncertainty in the line-shape normalization procedure [see Eq. (3)], due to the uncertainty in $\Gamma_{nat}$. We took our values of $\Gamma_{nat}$ from Niggli and Huber [22] and García and Campos [23]. These transition probabilities are lower by 30–50% than the values reported by Miles and Wiese [24], who estimate a 50% uncertainty in their values. (Uncertainties in the values reported in Refs. [22,23] are <20%.) However, the uncertainty in the $\Gamma_{nat}$ values affects our reported values of $k_{br}$ and $k_{shift}$ by only ~1% since the line shape remains essentially unchanged by variations of $\Gamma_{nat}$ ($\Gamma_{br} \gg \Gamma_{nat}$). On the other hand, the uncertainty in these $\Gamma_{nat}$ values directly affects the uncertainty in the excited-state atom number densities, derived from these measurements, since $n_{^3D_J}$ is inversely proportional to $\Gamma_{nat}$ [see Eq. (3)].

The main sources of error in the determination of $k_{br}$ arise from the $^3D_J$ density scaling process and the extraction of $\Gamma_{br}$ from the experimental line shapes. While the uncertainty in scaling the relative densities of any two scans is roughly 10–15%, the $f_{ij}$ scaling factors are multiplied together when scaling from the lowest metastable-state density curve to the highest. Thus, the scaling uncertainties increase with movement farther into the line wings, with a cumulative scaling uncertainty of 20–35% possible depending on the number of scans needed to construct the line shape. This is most dramatic in the lower-pressure data where typically five or even six scans were needed to map the line shape, as opposed to only three or four at higher buffer-gas pressure. (This effect can be seen in Fig. 6, where the fit in the far wings of the low-pressure curve is clearly worse than that for higher pressures.) Also, pressure broadening has a larger effect in the high-pressure scans where even the line core becomes Lorentzian. As a result, the more accurate line-core data contribute to the determination of $\Gamma_{br}$ for higher pressures. Thus, the uncertainty in $\Gamma_{br}$ for the higher-pressure data is much reduced due to the elimination of the scaling-factor uncertainties.

The mapping of the density-independent line shape is relevant to a variety of planned experiments. In the limit of weak pumping, we can measure $k_\nu$ at a single frequency and use our constructed absolute curves of $k_\nu/n_{^3D_J}$ to determine the corresponding metastable-level density. We have also used a pulsed dye laser to pump the $6s^2\ ^1S_0 \rightarrow 6s6p\ ^3P_1^\circ$ transition. Under these conditions, we can study the time-dependent populations in the metastable $6s5d\ ^3D_J$ levels by recording time-resolved cw probe laser transmission. (Details of this technique are planned to be presented in a forthcoming publication [25].) With these pulsed data, we can compare the line shapes measured in the low-power (cw) case (presented here) with those measured in the high-power (pulsed) case to test for intensity-dependent changes in the line shape (for exam-

ple, due to Stark broadening caused by multiphoton ionization). Preliminary comparisons of this type indicate that the line shape mapped with the pulsed pump laser can be fitted very well by a Voigt function using the appropriate value of $k_{br}$ measured in this work. Analysis of the pulsed line shapes is proceeding, and is planned to be presented soon.

Finally, we wish to comment on the $^3D_J$ level populations that were measured in this work. Typical ground-state number densities in this experiment were on the order of $10^{13}$ cm$^{-3}$. However, as was mentioned previously, the order-of-magnitude uncertainty in the noble-gas broadening rate coefficients do not allow us to determine an accurate ground-state number density using the equivalent width method. For each of the metastable $^3D_J$ states, the number density obtained through the line-shape normalization was typically $> 10^{12}$ cm$^{-3}$, when full power of the weak cw diode laser was incident on the barium vapor, although large uncertainties (discussed previously in this section) prevent us from determining a more accurate value. Thus, while it seems apparent that an appreciable fraction of the ground-state atoms are, in fact, being optically pumped into (and presumably trapped in) these metastable levels, an accurate estimate of the total barium population that is residing in these levels is not possible at the present time. Still, the barium $^3D_J$ levels represent an interesting energy-storage system. Further experiments on the population and depopulation mechanisms of these levels are in progress in our laboratory.

## ACKNOWLEDGMENTS

The authors are grateful to Dr. Wei-Tzou Luh for his work on this experiment during its early stages and to Ms. Zeina Jabbour for many useful discussions. We also gratefully acknowledge financial support for this work provided by the U.S. Army Research Office (Grant No. DAAL03-89-K-0171) and the National Science Foundation (Grant No. PHY-9119498).

[1] N. P. Penkin and L. N. Shabanova, Opt. Spektrosk. **25**, 795 (1968) [Opt. Spectrosc. (USSR) **25**, 446 (1968)].
[2] G. V. Zhuvikin, N. P. Penkin, and L. N. Shabanova, Opt. Spektrosk. **46**, 1135 (1979) [Opt. Spectrosc. (USSR) **46**, 642 (1979)].
[3] H. Harima, K. Tachibana, and Y. Urano, J. Phys. B **15**, 3679 (1982).
[4] W. J. Alford, N. Anderson, K. Burnett, and J. Cooper, Phys. Rev. A **30**, 2366 (1984).
[5] E. Kuchta, R. J. Alvarez, Y. H. Li, D. A. Krueger, and C. Y. She, Appl. Phys. B **50**, 129 (1990).
[6] J. L. Carlsten, J. Phys. B **7**, 1620 (1974).
[7] S. G. Schmelling, Phys. Rev. A **9**, 1097 (1974).
[8] P. G. Whitkop and J. R. Wiesenfeld, J. Chem. Phys. **72**, 1297 (1980).
[9] J. Migdalek and W. E. Baylis, Phys. Rev. A **42**, 6897 (1990).
[10] A. F. Bernhardt, Appl. Phys. **9**, 19 (1976).
[11] I. I. Klimovskii, P. V. Minaev, and A. V. Morozov, Opt. Spektrosk. **50**, 847 (1981) [Opt. Spectrosc. (USSR) **50**, 464 (1981)].
[12] C. R. Vidal and J. Cooper, J. Appl. Phys. **40**, 3370 (1969).
[13] R. E. Honig and D. A. Kramer, RCA Rev., p. 285 (June 1969).
[14] C. R. Vidal and F. B. Haller, Rev. Sci. Instrum. **42**, 1779 (1971).
[15] M. Gustavsson, I. Lindgren, G. Olsson, A. Rósen, and S. Svanberg, Phys. Lett. A **62**, 250 (1977).
[16] P. Grundevik, M. Gustavsson, G. Olsson, and T. Olsson, Z. Phys. A **312**, 1 (1983).
[17] A. Corney, *Atomic and Laser Spectroscopy* (Clarendon, Oxford, 1977).
[18] A. G. C. Mitchell and M. W. Zemansky, *Resonance Radiation and Excited Atoms* (Cambridge University Press, Cambridge, 1934).
[19] D. G. Hummer, Mem. R. Astron. Soc. **70**, 1 (1965).
[20] *Handbook of Chemistry and Physics, 71st ed.*, edited by D. L. Lide (CRC Press, Boca Raton, FL, 1990).
[21] M. Kötteritzsch, W. Gries, and A. Hese, J. Phys. B **25**, 913 (1992).
[22] S. Niggli and M. C. E. Huber, Phys. Rev. A **35**, 2908 (1987).
[23] G. García and J. Campos, J. Quant. Spectrosc. Radiat. Transfer **42**, 567 (1989).
[24] B. M. Miles and W. L. Wiese, At. Data **1**, 1 (1969).
[25] E. Ehrlacher and J. Huennekens (unpublished).